

The globular cluster systems of 54 Coma ultra-diffuse galaxies: statistical constraints from *HST* data

N. C. Amorisco^{1,2*}, A. Monachesi¹, S. D. M. White¹

¹*Max Planck Institute for Astrophysics, Karl-Schwarzschild-Strasse 1, 85748 Garching, Germany,*

²*Institute for Theory and Computation, Harvard-Smithsonian Center for Astrophysics, 60 Garden St., MS-51, Cambridge, MA 02138, USA*

7 October 2016

ABSTRACT

We use data from the *HST* Coma Cluster Treasury program to assess the richness of the Globular Cluster Systems (GCSs) of 54 Coma ultra-diffuse galaxies (UDGs), and hence to constrain the virial masses of their haloes. For 18 of these the half-light radius exceeds 1.5 kpc. We use a maximum-likelihood method to take account of the high contamination levels. UDG GCSs are poor: for 14 of the largest 18, $N_{\text{GC}} < 29$ with 90% confidence, $N_{\text{GC}} \leq 46$ for the remaining 4. From a stacked analysis of the 18 largest UDGs we estimate $\langle N_{\text{GC}} \rangle = 4.9_{-3.3}^{+4.3}$ (median, 10 and 90% quantiles); the corresponding number for the complementary 36 systems is $\langle N_{\text{GC}} \rangle = 0.8_{-0.6}^{+0.9}$. These results strongly suggest that most Coma UDGs have low-mass haloes. Their GCSs do not display significantly larger richnesses than nearby dwarf galaxies of similar stellar mass.

Key words: galaxies: dwarf — galaxies: structure — galaxies: formation — galaxies: haloes — galaxies: clusters

1 INTRODUCTION

Ultra-diffuse galaxies (UDGs) are a population of low-surface brightness systems (effective surface brightness $\langle \mu \rangle_r \gtrsim 24$ mag/arcsec²) with stellar masses typical of dwarf galaxies ($7 \lesssim \log M_*/M_\odot \lesssim 9$). Ubiquitous in nearby galaxy clusters (van Dokkum et al. 2015; Koda et al. 2015; Muñoz et al. 2015; van der Burg et al. 2016; Mihos et al. 2015), UDGs have also been found outside cluster environments (Martinez-Delgado et al. 2016; Roman & Trujillo 2016). They appear as roundish featureless spheroids (e.g. Yagi et al. 2016), which extend the red sequence of cluster galaxies in the colour-magnitude diagram into the regime of dwarf galaxies (Koda et al. 2015; van der Burg et al. 2016), with hints of a trend to bluer colours in less dense environments (Roman & Trujillo 2016).

Interest in this population has been sparked by the proposal that their halo mass could be much larger than suggested by their stellar mass (van Dokkum et al. 2015; Koda et al. 2015; van Dokkum et al. 2016). According to this proposal, the largest UDGs (e.g. half-light radii $\gtrsim 1.5$ kpc) would be hosted by Milky Way (MW) mass haloes rather than by haloes with masses below or similar to that of the Large Magellanic Cloud (LMC). In either case, UDGs are highly dark matter dominated systems (van Dokkum et al. 2015; Beasley et al. 2016; Amorisco & Loeb 2016; van Dokkum et

al. 2016). However, if hosted by MW mass haloes, they are strong outliers from the $M_* - M_{\text{vir}}$ relation: this would require their formation pathway to differ fundamentally from that of ‘normal’ haloes of the same total mass, which are thought to be the most efficient at converting gas into stars (e.g. Guo et al. 2010; Behroozi et al. 2013; Moster et al. 2013, and references therein). As suggested by a simplistic Λ CDM framework, this is not necessary. A scenario in which UDGs are the low surface brightness tail of the abundant population of dwarf galaxies can capture the abundances and size distribution of cluster UDGs in detail (Amorisco & Loeb 2016). In addition, if hosted by low mass haloes, internal stellar feedback might provide a promising way to ‘expand’ them to large sizes (Di Cintio et al. 2016), both inside and outside clusters, without the need for *ad hoc* mechanisms to make them depart so significantly from the $M_* - M_{\text{vir}}$ relation.

Unfortunately, only three UDG halo mass measurements are available so far to inform this discussion. These are indirect measurements, based either on the richness of the globular cluster system (GCS), used as a proxy for halo mass, or on an extrapolation to the virial radius of a dynamical mass measurement (Beasley et al. 2016; Beasley & Trujillo 2016; Peng & Lim 2016; van Dokkum et al. 2016). Both techniques have their limitations. The approximate linearity of the relation between the GCS richness and halo virial mass is supported by a solid pool of evidence (e.g., Harris et al. 2013; Hudson et al. 2014; Forbes et al. 2016,

* E-mail: nicola.amorisco@cfa.harvard.edu

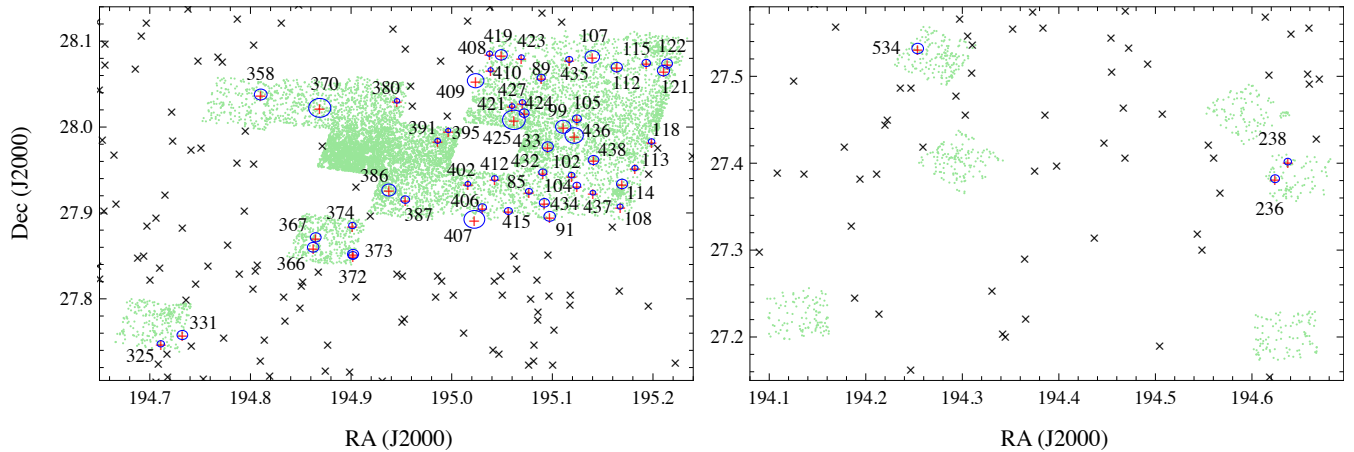


Figure 1. A composite of the *HST*/ACS fields observed as part of the Coma Cluster Treasury program, together with the Coma UDGs from Yagi et al. (2016), shown as black and red cross symbols. Green points are candidate GCs selected from the Hammer et al. (2010) catalog, as described in Sect. 2.1. The 54 UDGs whose centers fall within the observed *HST* fields are marked in red, their size is shown by a blue circle (with a radius of $6 \times R_S$), and their ID number in the Yagi et al. (2016) catalog is displayed.

and references therein), but the mean conversion factor remains uncertain (Harris et al. 2015; Zaritsky et al. 2016; Georgiev et al. 2010, hereafter G10) and might not apply to these unusual systems. Dynamical measurements, however, do not guarantee higher precision, as the extrapolation from the galaxy’s half-light radius (e.g. Walker et al. 2009; Wolf et al. 2010; Amorisco & Evans 2011; Campbell et al. 2016) to the virial radius is very substantial.

In this Letter, we set out to solidify the sample of virial mass estimates for UDGs by enlarging it by over an order of magnitude. We use imaging data from the *HST* Coma Cluster Treasury program to constrain the richness of the GCS of 54 Coma UDGs. With respect to ground-based data, *HST*/ACS data are ideal to disentangle candidate GCs from most background galaxies (e.g., Peng et al. 2011; Beasley & Trujillo 2016; Peng & Lim 2016). However, the poor UDG GCSs and the high contamination imply that a fully statistical framework has to be adopted to gather reliable constraints. Sect. 2.1 describes the data; Sect. 2.2 sets out the maximum-likelihood approach we employ, and Sect. 3 presents our results. Sect. 4 lays out the Conclusions.

2 OBSERVATIONS AND METHODS

We use the compilation of 854 Coma UDGs presented by Yagi et al. (2016, hereafter Y16), based on Subaru Suprime Cam archival data analysed in Koda et al. (2015). These are selected to have $\langle \mu \rangle_R < 24$ mag/arcsec² and a stellar half light radius ≥ 0.7 kpc. Among these, we select those UDGs whose centers lie within the footprint of the Coma Cluster Treasury program, which we use to explore the properties of their GCSs. There are 54 such UDGs. Their locations are displayed in Fig. 1, together with their ID numbers in the Y16 catalog. We adopt half-light radii R_S from the single Sersic fits presented by Y16. Where these were not deemed reliable, for example, because of light from nearby systems, we adopt the listed values returned by SExtractor.

2.1 Candidate GC selection

We cross-correlate the position of the Y16 UDGs with the catalog of the *HST*/ACS Coma Cluster Treasury program (CCTp) presented by Hammer et al. (2010, hereafter H10). This lists all SExtractor sources detected in the deep *F814W* images, as well as the measurements for the *F475W* images, and we use it to select GC candidates (GCCs) within the footprint of the survey. AB magnitude system photometry is available at different apertures: we use the 4 pixel radius aperture ($0.''2$) and apply the aperture corrections from Sirianni et al. (2005). We correct magnitudes for Galactic extinction following Schlafly & Finkbeiner (2011), using the $E(B-V)$ reddening values from Schlegel et al. (1998). The *F814W*–band photometry is 80% and 50% complete at 26.8 and 27.3, respectively (H10 and Peng et al. 2011). This defines our completeness function S_{814} , for which we adopt the functional form suggested by Salinas et al. (2015, eqn. 3, resulting in $\alpha = 1.5$).

HST/ACS imaging ($0.''05/\text{pixel}$) is ideal to disentangle GCCs (point sources at the distance of Coma) from most background galaxies, which appear resolved. We first select objects flagged as ‘point source’ in the H10 catalog (FLAGS_OBJ=1). Following Peng et al. (2011), we then define the concentration index C_{4-10} as the difference in magnitudes between a 4- and a 10-pixel radius aperture. The locus of point sources is at $C_{4-10} = 0.13$. Using the concentration index and *F814W* magnitudes we generate our sample of GCCs, including all objects within ± 0.2 mag of the C_{4-10} locus and with *F814W* < 27.3 . In addition, we apply a colour cut $0.5 < F475W - F814W < 1.5$ to isolate GCs from compact red galaxies (Peng et al. 2011; Beasley & Trujillo 2016), and we impose a bright magnitude limit of *F814W* < 22 to avoid foreground MW stars and saturated pixels (H10). The final catalog contains ~ 12000 GCCs¹.

¹ We estimate that 42 sources in our catalog might be duplicate detections from coadding the catalogs of the 25 *HST*/ACS fields observed in the CCTp, which is negligible.

2.2 Statistical analysis

As shown by Peng et al. (2011) using the same data, the Coma cluster possesses an abundant population of intra-cluster GCs (ICGs), and several tens of background galaxies per ACS field survive the selection just described. Although the CCTp data is 50% complete at the turnover of the GC luminosity function (GCLF) of dwarf ellipticals ($F814W = 27.33$ Miller & Lotz 2007; Peng et al. 2011; Beasley & Trujillo 2016), visual inspection rarely reveals any apparent over-density of GCCs near the UDG centers. These over-densities are readily seen by eye at the locations of high surface brightness Coma galaxies. On average, UDGs have poor GCSs relative to the background, implying that we are forced to adopt a statistical approach to constrain their richness (N_{GC}). Given (i) the lack of evident overdensities, (ii) the properties of the background and (iii) the magnitude completeness function, we can extract constraints on N_{GC} .

We isolate the GCCs in the vicinity of each UDG, and model them as the superposition of a population of contaminants and of a population of GCs physically associated with the UDG. In absence of close luminous galaxies, we model all GCCs within $35 \times R_S$ from the UDG's center. This is a compromise between getting better statistics for the contaminants, and modelling their spatial distribution as locally uniform, with surface density Σ_c . The spatial distribution of the UDG GCS is modelled with either a Plummer or an exponential profile $\Sigma(r)$, whose half-count radius R_h is a free parameter. Following Walker & Peñarrubia (2011) and Amorisco et al. (2014), the probability of observing a sample of N GCCs at distances \mathbf{r}_i from the UDG is

$$\mathcal{L} = \prod_i^N \left[f \frac{S_{sp}(\mathbf{r}_i) \Sigma(r_i, R_h)}{\int S_{sp}(\mathbf{r}) \Sigma(r, R_h)} + (1 - f) \frac{S_{sp}(\mathbf{r}_i)}{\int S_{sp}} \right], \quad (1)$$

which is the likelihood function for the free parameters f and R_h/R_S (Σ_c cancels out). Here, (i) $S_{sp}(\mathbf{r})$ is the spatial selection function, which takes into account that the area available to study might be limited by the edges of the footprint; (ii) f is the fraction of the N GCCs to be associated with the UDG; (iii) integrals extend over the studied areas.

To ensure that our results are not strongly model dependent, we explore the following set of models:

- *model 1*: Plummer distribution, $0.5 < R_h/R_S < 3.5$;
- *model 2*: as *model 1*, enforcing a Gaussian prior on the ratio R_h/R_S , $R_h/R_S = 1.8 \pm 0.7$ (Kantha et al. 2014; Beasley et al. 2016; Peng & Lim 2016);
- *model 3*: as *model 1*, enforcing a Gaussian prior on the GCLF of the UDG GCS, $F814W = 27.33 \pm 1.1$ mag;
- *model 4*: exponential distribution, $0.5 < R_h/R_S < 3.5$.

In all cases, a uniform prior is imposed on $0 \leq f \leq 1$ and inference on N_{GC} is obtained from the inference on f by correcting the latter for both spatial and magnitude selections:

$$N_{GC,j} = N f_j \times \frac{\int \Sigma(r, R_{h,j})}{\int S_{sp}(\mathbf{r}) \Sigma(r, R_{h,j})} \frac{\int \mathcal{G}(F814W)}{\int S_{814} \mathcal{G}(F814W)}, \quad (2)$$

where j runs over the Monte Carlo chains, \mathcal{G} is the GCLF and S_{814} is the completeness function defined in Sect. 2.1. The turnover and spread of the GCLF vary with galaxy mass, becoming respectively fainter and tighter in dwarf galaxies (e.g. Jordán et al. 2007). We conservatively adopt a

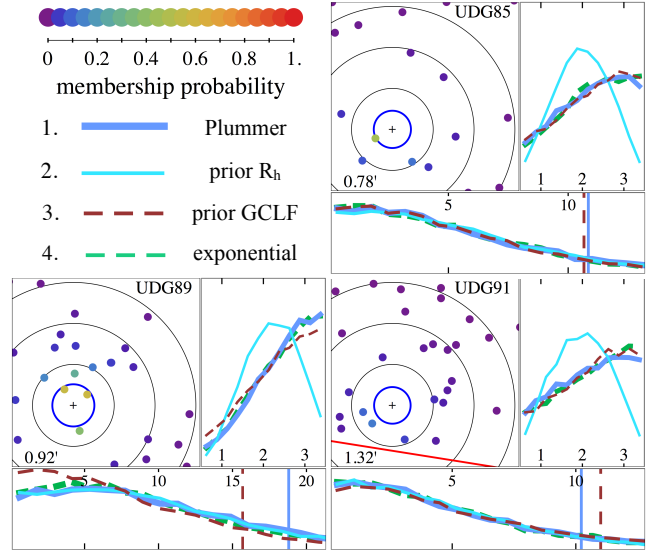


Figure 2. A summary of the statistical constraints on the GCSs of the first 3 Coma UDGs in the footprint of the CCTp. A complete version of this Figure is available [here](#). For each UDG, the upper-left panel shows a zoom of Fig. 1, with size $l \times l$, with l indicated in the lower left of the panel. Black concentric circles display $\{5, 10, 15\} \times R_S$, the stellar half-light radius of the UDG. The blue circle indicates the median half-counts radius R_h of the GCS we infer from *model 1*. Where visible, red lines show the edge of the footprint, or areas excluded due to bright galaxies. Dots are candidate GCs, color-coded by the probability of membership in the UDG, as shown in the legend. The upper-right panels display inferences (as posterior probability distributions) obtained for the ratio R_h/R_S using our models, as indicated in the legend. The lower panels show the associated inferences for the GCS richness, N_{GC} ; vertical lines indicate 90% quantiles from *model 1* and *3*.

dwarf-like GCLF (e.g., Miller & Lotz 2007; Peng et al. 2009, G10, mean and spread as in *model 3*), as this implies a larger correction through eqn. 2.

3 RESULTS

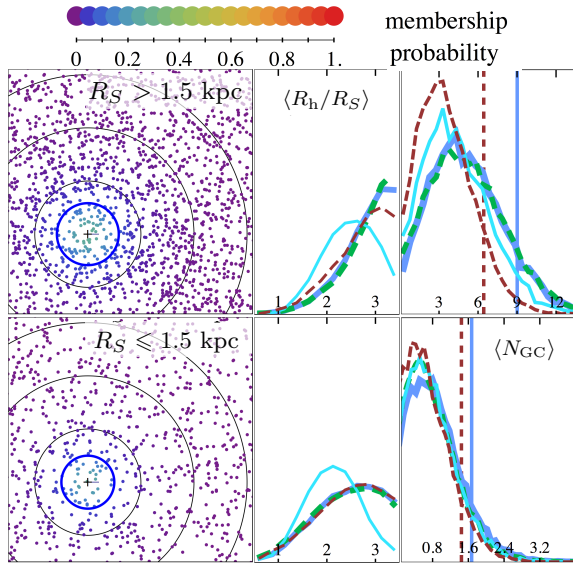
We apply the analysis described above to each UDG in our sample individually, and then to (i) the stack of the 18 systems with $R_S > 1.5$ kpc (and the stack of the complementary set of 36); (ii) the stack of the 18 systems with $\log M_*/M_\odot > 7.5$ (and the stack of the complementary set of 36).

3.1 Analyses on individual systems

Results for all our 54 UDGs are presented in Fig. 2 and Table 1. For each UDG, Fig. 2 displays posterior probability distributions for R_h/R_S (upper-right panels) and N_{GC} (lower panels). Quantiles for the N_{GC} distributions (10, 50 and 90%) are collected in Table 1. Zooms of Fig. 1 centered on the UDG locations (upper-left panels) show all GCCs, colour-coded according to their probability of membership to the UDG GCS (from *model 1*). As mentioned earlier, most cases show no obvious over-density of sources close to the center of the UDG, hence the paucity of high-probability

Table 1. Summary of the statistical constraints from our models, in terms of {10%, 50%, 90%} quantiles for all listed quantities. We list our 4 stacks and the first 3 Coma UDGs in the footprint of the CCTp. A complete version of this Table is available [here](#).

stack or ID	R_s kpc	$\log M_*$ M_\odot	R_h/R_s	N_{GC}	M_{vir} $10^{10} M_\odot$	N_{GC}	N_{GC}	N_{GC}
			model 1	model 1	model 1	model 2	model 3	model 4
$R_S > 1.5$ kpc	1.99	7.64	{2.1, 2.9, 3.4}	{1.7, 4.9, 9.0}	{0.5, 1.4, 2.5}	{1.3, 4.1, 7.9}	{1.0, 3.3, 6.4}	{1.6, 4.9, 9.2}
$R_S \leq 1.5$ kpc	1.03	7.08	{1.5, 2.5, 3.3}	{0.2, 0.8, 1.7}	{0.1, 0.2, 0.5}	{0.2, 0.7, 1.6}	{0.1, 0.6, 1.4}	{0.2, 0.7, 1.6}
$\log M_* > 7.5$	1.80	7.79	{1.8, 2.7, 3.3}	{0.9, 3.3, 6.5}	{0.3, 0.9, 1.8}	{0.8, 2.8, 5.7}	{0.4, 1.9, 4.2}	{0.9, 3.2, 6.3}
$\log M_* \leq 7.5$	1.13	7.01	{1.7, 2.7, 3.3}	{0.3, 1.3, 2.7}	{0.1, 0.4, 0.8}	{0.3, 1.1, 2.4}	{0.4, 1.2, 2.4}	{0.3, 1.3, 2.7}
85	0.94	7.2	{1.0, 2.3, 3.2}	{0.8, 4.2, 10.8}	{0.2, 1.2, 3.0}	{0.8, 4.4, 10.7}	{0.8, 4.1, 10.7}	{0.8, 4.2, 10.6}
89	1.10	7.5	{1.4, 2.6, 3.3}	{1.8, 8.1, 18.8}	{0.5, 2.3, 5.3}	{1.7, 8.1, 18.4}	{1.2, 6.3, 15.7}	{1.7, 7.6, 17.8}
91	1.58	6.8	{1.0, 2.2, 3.2}	{0.7, 3.8, 10.2}	{0.2, 1.1, 2.9}	{0.7, 3.8, 9.7}	{0.8, 4.0, 11.0}	{0.7, 3.8, 10.3}

**Figure 3.** Analysis on the stacks $R_S > 1.5$ kpc (top row) and $R_S \leq 1.5$ kpc (bottom row). Line styles are as in Fig. 2. Zooms display all GCCs in the stacks.

members. In several instances, the surface density of contaminants is such that even GCCs located within a few R_S from the UDG’s center cannot be considered physically associated beyond doubt.

We find no appreciable difference between constraints obtained through different model assumptions or using priors. We have also explored using a more restrictive catalog of GCCs (applying cuts as from [Peng et al. 2011](#)), which reduces the sample to ~ 5400 . Results remain consistent, although, as the deeper catalogue best probes the statistics of the contaminant population, we deem the inferences extracted from it more reliable.

As seen in Fig. 2, most posteriors on N_{GC} increase almost all the way to $N_{GC} = 0$: only 19 of our UDGs have $N_{GC,5} > 1$, i.e. are associated with more than 1 GC at 95% confidence. This result depends critically on the prior distribution adopted for f , and a large fraction of these detections are not confirmed when imposing a uniform prior on $\log f$ (rather than on f). Therefore, we stress that lower limits and medians obtained for individual systems should not be interpreted as measurements. However, we can extract reliable individual upper bounds. Even if we adopt the loosest

90% upper limits among those returned by our 4 models – as in the abstract – these show our 54-strong sample to be made of dwarfs. We follow [Harris et al. \(2015\)](#), and interpret our results on N_{GC} as inferences on the virial mass of the studied UDGs. We adopt the conversion factor suggested by G10, who used *HST* data and dynamical mass estimates of nearby dwarf galaxies to calibrate the following mean relation

$$M_{vir} \equiv \frac{1}{\eta} M_{GCS} \equiv N_{GC} \frac{\langle M_{GC} \rangle}{\eta} \sim N_{GC} \frac{1.69 \times 10^5 M_\odot}{6 \times 10^{-5}}, \quad (3)$$

where M_{GCS} is the mass of the GCS and $\langle M_{GC} \rangle$ is the mass corresponding to the turnoff of the GCLF. It is reassuring that independent studies with different systematics agree on this calibration² to about a factor ~ 2 (e.g., [Harris et al. 2015](#); [Zaritsky et al. 2016](#); [Forbes et al. 2016](#)). Sticking to the results of *model 1*, 49 of our 54 of our UDGs have $M_{vir,90} < 10^{11} M_\odot$ (90% quantile). Of the 18 UDGs with $R_S > 1.5$ kpc, 14 have $M_{vir,90} < 10^{11} M_\odot$, with the remaining 4 satisfying $M_{vir,90} < 1.3 \times 10^{11} M_\odot$. We also note that systems in the latter group of 4 are characterised by especially high density of contaminant densities (likely ICGs and/or GCs from the nearby N4889), which substantially inflate the uncertainties (see, for example, the system ID 425 in the complete version of Fig. 2). Table 1 provides the conversion of the results of *model 1* to virial mass for all 54 UDGs.

3.2 Analyses on stacks

The combination of the paucity of physically associated GCs and the $\sim \sqrt{N}$ Poisson uncertainty deriving from the dominant background counts implies we can only extract upper bounds for individual systems. We can partially circumvent this and improve our statistics by stacking: we combine UDGs based on their size, stacking the 18 systems with $R_S > 1.5$ kpc, or based on their stellar mass, combining the 18 systems with $\log M_* > 7.5$, as well as the complementary samples of 36. This allows us to extract information on the *average* richness of UDG GCSs, $\langle N_{GC} \rangle$.

Fig. 3 illustrates the results obtained for the stacks based on size, and Table 1 lists quantiles for both analyses. As shown by the posterior probability distributions on

² Massive galaxies lie on the relation $M_{vir} \sim N_{GC} (2.4 \times 10^5 M_\odot / 4 \times 10^{-5})$; the halo-to-halo scatter in dwarfs appears wider than this difference (G10).

$\langle N_{GC} \rangle$ in Fig. 3, this strategy allows us to extract significant measurements for the stack of the largest UDGs (as well as for the stack of the most luminous). The average richness $\langle N_{GC} \rangle$ remains as typical for dwarf galaxies: independently of model assumptions, our 18 UDGs with $R_S > 1.5$ kpc have $\langle N_{GC,50} \rangle \sim 5$, which corresponds to an average halo mass of $\langle M_{vir,50} \rangle \sim 1.4 \times 10^{10} M_\odot$.

4 DISCUSSION AND CONCLUSIONS

UDGs are a startling class of systems because of the apparent mismatch between their stellar mass and size, which results in very high dark matter fractions within their optical radii (Beasley et al. 2016; Beasley & Trujillo 2016; Peng & Lim 2016; van Dokkum et al. 2016), independently of whether they are hosted by dwarf or MW mass haloes. One aspect that has not been sufficiently highlighted so far is the almost perfect linearity of the relation between the abundance of UDGs in clusters and the cluster mass itself (van der Burg et al. 2016). This indicates that UDGs are an approximately constant fraction of cluster populations, bearing little additional dependence on the cluster richness, and by extension on local environment. In turn, this would suggest that the physical mechanism that gives UDGs their unusual properties may in fact have an *internal origin*, rather than being caused by interactions with the environment, as corroborated by the detection of UDGs outside cluster cores (Martinez-Delgado et al. 2016; Roman & Trujillo 2016).

There is no shortage of mechanisms proposed so far to form galaxies with the properties of UDGs, including (i) high angular momentum content of primordial origin (Amorisco & Loeb 2016); (ii) especially strong and prolonged stellar feedback (Di Cintio et al. 2016); (iii) premature quenching due to early infall onto the cluster (Yozin & Bekki 2015; van Dokkum et al. 2015); (iv) 2-body galaxy-encounters within the cluster itself (Baushev 2016; Burkert 2016). Among these, the first two are of internal origin, while the latter two require the external influence of a dense environment, in combination with early infall.

Our results show that most UDGs are hosted by dwarf mass haloes: we find no candidate for a massive MW-like halo. Beasley & Trujillo (2016) and Peng & Lim (2016) have suggested that, though hosted by LMC mass haloes, UDGs might still show signs of ‘failure’, having rich GCSs for their stellar mass. We explore this further in Fig. 4, by comparing our UDGs with nearby galaxies from the compilations of Harris et al. (2013, H13, grey rectangles) and G10 (green stars, from their Table 1). Galaxies from the G10 compilation include nearby dwarfs in groups or loose associations in which at least a GC has been observed. Dots with blue error-bars identify the measurements by Beasley et al. (2016) for VCC 1287 in Virgo; Peng & Lim (2016) and Beasley & Trujillo (2016) for DF17; van Dokkum et al. (2016) for DF44, which is a strong outlier in this plane (see also the analysis of Zaritsky 2016). Stellar masses are obtained assuming that $B - R \sim 1$ for the UDGs (Koda et al. 2015), and using morphological type as a proxy for colour within the H13 catalog. The uncertainty displayed in the top-left shows the difference between the masses inferred using the M/L relations of Zibetti et al. (2009) and Bell et al. (2003). For our 54 UDGs, downward arrows display individual upper

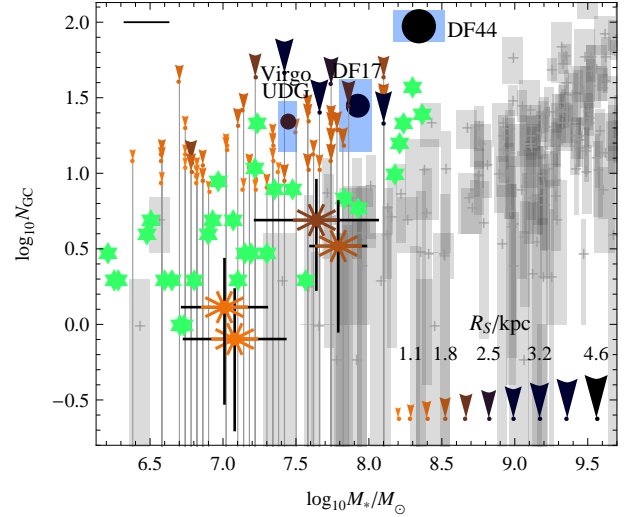


Figure 4. The richness of the GCS of ‘normal’ galaxies from the H13 catalog (grey rectangles), dwarf galaxies from G10 (green stars) and three Coma and Virgo UDGs from the literature (blue rectangles with full dots), compared to our sample of 54 Coma UDGs. Individual upper bounds (90% quantiles) are shown by downward arrows. Large asterisks show the results of our stacking analyses (medians with 10-90% quantile error-bar for N_{GC} ; mean with 1σ scatter for $\log M_*$). Symbols for all UDGs are colour-coded according to their stellar half-light radius.

bounds ($N_{GC,90}$ from *model 1*); large asterisks with error-bars show results obtained from our stacking analyses. UDG symbols are colour-coded according to the stellar half-light radius. The large asterisks show that more luminous (and/or larger) UDGs have on average richer GCSs, a result that is also hinted to by the individual upper bounds. While we cannot exclude that some GCs have been lost as a result of cluster tides, our UDGs do not appear to deviate from the galaxies in the H13 catalog, or from the sample of dwarf galaxies of G10: we can rule out large systematic discrepancies in the richness of their GCSs. On a sample of 54 systems, all the data agree that GCSs of UDGs have very similar richnesses to those of ‘normal’ dwarfs of similar stellar mass. This strongly suggests that their halo masses are also similar.

ACKNOWLEDGEMENTS

NA and AM acknowledge stimulating discussions with Chervin Laporte. NA thanks Adriano Agnello, Mike Beasley and Abraham Loeb for comments on an early version of this draft.

REFERENCES

- Amorisco, N. C., & Evans, N. W. 2011, MNRAS, 411, 2118
- Amorisco, N. C., Evans, N. W., & van de Ven, G. 2014, Nat, 507, 335
- Amorisco, N. C., & Loeb, A. 2016, MNRAS, 459, L51
- Baushev, A. N. 2016, arXiv:1608.04356
- Beasley, M. A., Romanowsky, A. J., Pota, V., et al. 2016, arXiv:1602.04002
- Beasley, M. A., & Trujillo, I. 2016, arXiv:1604.08024

- Behroozi, P. S., Wechsler, R. H., & Conroy, C. 2013, *ApJ*, 770, 57
- Bell, E. F., McIntosh, D. H., Katz, N., & Weinberg, M. D. 2003, *ApJS*, 149, 289
- Burkert, A. 2016, arXiv:1609.00052
- Campbell, D. J. R., Frenk, C. S., Jenkins, A., et al. 2016, arXiv:1603.04443
- Di Cintio, A., Brook, C. B., Dutton, A. A., et al. 2016, arXiv:1608.01327
- Forbes, D. A., Alabi, A., Romanowsky, A. J., et al. 2016, *MNRAS*, 458, L44
- Georgiev, I. Y., Puzia, T. H., Goudfrooij, P., & Hilker, M. 2010, *MNRAS*, 406, 1967
- Guo, Q., White, S., Li, C., & Boylan-Kolchin, M. 2010, *MNRAS*, 404, 1111
- Hammer, D., Verdoes Kleijn, G., Hoyos, C., et al. 2010, *ApJS*, 191, 143
- Harris, W. E., Harris, G. L. H., & Alessi, M. 2013, *ApJ*, 772, 82
- Harris, W. E., Harris, G. L., & Hudson, M. J. 2015, *ApJ*, 806, 36
- Hudson, M. J., Harris, G. L., & Harris, W. E. 2014, *ApJL*, 787, L5
- Jordán, A., McLaughlin, D. E., Côté, P., et al. 2007, *ApJS*, 171, 101
- Kartha, S. S., Forbes, D. A., Spitler, L. R., et al. 2014, *MNRAS*, 437, 273
- Koda, J., Yagi, M., Yamanai, H., & Komiyama, Y. 2015, *ApJL*, 807, L2
- Mackey, A. D., & Gilmore, G. F. 2003, *MNRAS*, 338, 85
- Martinez-Delgado, D., Laesker, R., Sharina, M., et al. 2016, arXiv:1601.06960
- Mihos, J. C., Durrell, P. R., Ferrarese, L., et al. 2015, *ApJL*, 809, L21
- Miller, B. W., & Lotz, J. M. 2007, *ApJ*, 670, 1074
- Moster, B. P., Naab, T., & White, S. D. M. 2013, *MNRAS*, 428, 3121
- Muñoz, R. P., Eigenthaler, P., Puzia, T. H., et al. 2015, *ApJL*, 813, L15
- Peng, E. W., Jordán, A., Blakeslee, J. P., et al. 2009, *ApJ*, 703, 42
- Peng, E. W., Ferguson, H. C., Goudfrooij, P., et al. 2011, *ApJ*, 730, 23
- Peng, E. W., & Lim, S. 2016, *ApJL*, 822, L31
- Roman, J., & Trujillo, I. 2016, arXiv:1603.03494
- Salinas, R., Alabi, A., Richtler, T., & Lane, R. R. 2015, *AA*, 577, A59
- Schlafly, E. F., & Finkbeiner, D. P. 2011, *ApJ*, 737, 103
- Schlegel, D. J., Finkbeiner, D. P., & Davis, M. 1998, *ApJ*, 500, 525
- Sirianni, M., Jee, M. J., Benítez, N., et al. 2005, *PASP*, 117, 1049
- van der Burg, R. F. J., Muzzin, A., & Hoekstra, H. 2016, arXiv:1602.00002
- van Dokkum, P. G., Abraham, R., Merritt, A., et al. 2015, *ApJL*, 798, L45
- van Dokkum, P., Abraham, R., Brodie, J., et al. 2016, *ApJL*, 828, L6
- Yagi, M., Koda, J., Komiyama, Y., & Yamanai, H. 2016, *ApJS*, 225, 11
- Yozin, C., & Bekki, K. 2015, *MNRAS*, 452, 937
- Walker, M. G., Mateo, M., Olszewski, E. W., et al. 2009, *ApJ*, 704, 1274
- Walker, M. G., & Peñarrubia, J. 2011, *ApJ*, 742, 20
- Wolf, J., Martinez, G. D., Bullock, J. S., et al. 2010, *MNRAS*, 406, 1220
- Zaritsky, D., Crnojević, D., & Sand, D. J. 2016, *ApJL*, 826, L9
- Zaritsky, D. 2016, arXiv:1609.08169
- Zibetti, S., Charlot, S., & Rix, H.-W. 2009, *MNRAS*, 400, 1181